LBL-35335
UC-419

Lawrence Berkeley Laboratory
UNIVERSITY OF CALIFORNIA

Accelerator & Fusion
Research Division

ILSE Combiner Study

K. Hahn

March 1994

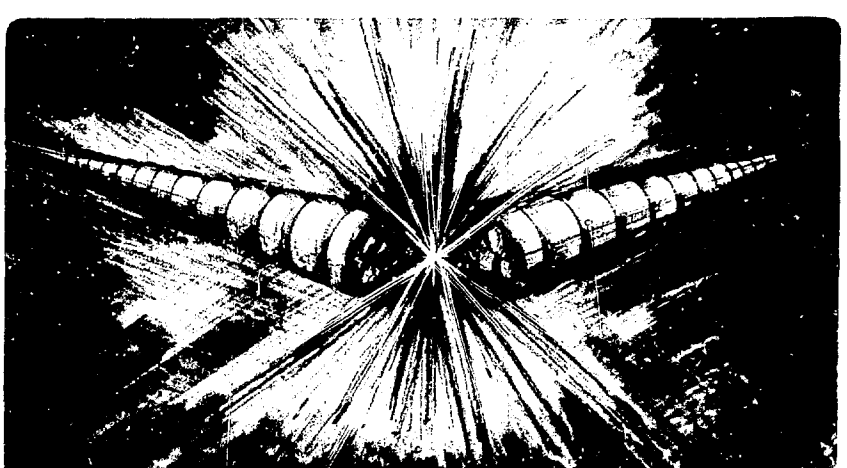

Prepared for the U.S. Department of Energy under Contract Number DE-AC03-76SF00098

LBL-35335
HIFAN-621
UC-419

ILSE Combiner Study

Kyoung Hahn

Lawrence Berkeley Laboratory
University of California
Berkeley, CA 94720

March 1994

* This work is supported by the Director, Office of Energy Research, Office of Fusion Energy, U.S. Department of Energy, under Contract No. DE-AC03-76SF00098.

ILSE Combiner Study
by
Kyoung Hahn

1 Introduction

In a heavy ion inertial fusion (HIF) driver, the beam energy and current are increased several orders of magnitude from the injector to the final focus system. At low and high energy stages of the driver, electrostatic and magnetic focusing transport channels, respectively, can be used. At the electric-to-magnetic transition point, the beams may be combined to reduce the transverse dimensions of the system, which could have significant impact on the driver cost.[1] In a presently envisioned combiner, four beams are brought together transversely into a single transport channel. A matching section follows the combiner in order to provide a smooth transition to the subsequent magnetic transport channel.

This report summarizes a conceptual design study of possible combiner configurations for the proposed Induction Linac Systems Experiment (ILSE). The conceptual design study includes subjects such as the expected technical difficulties, predicted emittance growth, particle loss, effect of geometric and chromatic aberrations, and the sensitivity of emittance growth on the initial beam position and angle errors.

The transverse emittance will inevitably increase by at least a factor of two in a "Liouvillian" stacking system, in which no "hole" in the phase space are produced. A further increase of the emittance can be deduced from the geometric dilution due to incomplete filling in the phase space, which makes the effective volume larger. In addition, incomplete filling in configuration space increases the emittance even further as the beam evolves into the quasi-equilibrium distribution due to the non-linear forces from space charge. This last cause is most important in combining beams of HIF interest, which are space-charge dominated. Emittance growth can be minimized by reducing the empty space between the beams. Various geometric and chromatic aberrations can further increase the emittance, and these effect should be minimized in a proper combiner design. Since the distance between the electrodes are less at the end of the combiner, the electrical breakdown limit must be carefully tested, especially for the combined function quadrupole elements, since the bending and quadrupole fields are of the same sign at some locations. Further care should be taken to *minimize multipole fringe fields which can increase emittance and cause particle* loss. A part of the beam will form a "halo" surrounding the main body of the beam, so some scraping off before the last element of the combiner could be used to reduce the danger of electrical breakdown.

[1] There are other driver designs, without the transverse beam combination, which introduce superconducting magnets early, at low-energy stage.

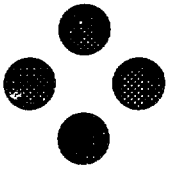

Figure 1: Symmetric configuration.

The main goals of the present conceptual design study are to minimize both the predicted emittance growth and the anticipated technical difficulties for detailed design. In the next two sections, specific combiner design studies are described for the symmetric and the "stonehenge" configurations. The symmetric combiner is conceptually simpler due to its four-fold symmetry. The stonehenge configuration has a better beam packing ratio, which resulted in a smaller emittance; however, the geometry requires complicated "wire cage" electrodes, which are technically more difficult, to generate required field.

In the course of the study a two dimensional particle-in-cell code HIBEAM has been developed by the author and used extensively to test the design criteria. This code is briefly described.

2 Merging configurations

At the end of the combiner beams may emerge in one of the two basic configurations, stonehenge and symmetric, which have two and four fold symmetries, respectively. Other possible configurations have been found to have high emittance growth for a fixed minimum separation and were therefore not studied in detail.

Among three possible symmetric merging configurations, the round beam shape configuration is chosen [Fig. 1], since it gives the best packing ratio, defined by the area ratio occupied by the beam to the total combiner cross-section for a given clearance distance. In order to minimize geometric dilution of the phase space, the envelope slope and merging angles are minimized consistent with electrode standoff.

In order to increase the packing ratio even further, the "stonehenge" configuration [Fig. 2] is introduced. In a stonehenge configuration the beam edge-to-edge distance between the all neighboring beams is equal, which minimizes the empty void space among them. In order to minimize the geometric dilution, the elliptic beam shape is chosen where the envelope slope is zero. The merging angle is also chosen to be zero on a design orbit. However, a small merging angle could be tolerated, and even could be beneficial, since the space

Figure 2: Stonehenge configuration.

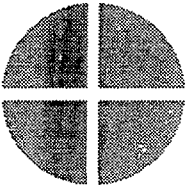

Figure 3: 'Pie' configuration. This configuration is of interest since no emittance growth can be achieved when the separation is zero.

charge contribution to emittance growth is less when the combined beam size is reduced.

A further increase of the packing ratio could be achieved by using non-elliptic beam shapes such as "Pie" configurations [Fig. 3] or hexagonal ones. These configurations can be driven by proper combinations of the multipoles by applying equal and opposite kicks at different z-locations. Note that the multipoles fields are divergence free, so that the density variation inside of the beam is zero to the leading order in kick strenght as long as the interval of the kick is less than the plasma period. Some simulation tests of this micro-shaping approach have been performed; a small improvement in emittance growth compared with the symmetric and stonehenge cases was found. However, the required large deformations of shape can not be achieved in this simple scheme.

3 Emittance growth

After the combining configuration is fixed, the emittance growth in the merging process is readily calculated.

The geometric dilution term for the four-to-one symmetric merging is given by

$$\epsilon_g^2 = (\frac{a^2+b^2}{2}+2d^2)[\frac{\epsilon_i^2}{2}(\frac{a^2+b^2}{a^2b^2})+2(\delta p)^2+\frac{1}{2}(a'^2+b'^2)]-[\frac{1}{2}(aa'+bb')+2d(\delta p)]^2$$

where d is the displacement of a beam center from the symmetry origin, δp is the convergence angle, $(a,\ b)$ are the the major and minor envelope radii of a beam, and ϵ_i is the initial emittance of the each of the four beams. In order to minimize the geometric dilution, the converging angle and the envelope slope as well as the beam-to-beam separation should be minimized.

The space charge contribution is estimated as follows [1];

$$\delta[\epsilon_n^2] = 2Qr^2\delta f$$

where $Q = \frac{\lambda_o}{\gamma mc^2}$, λ = line charge density, r is the envelope radius of the merged beam, and δf is a dimensionless profile factor depending on the beamlet arrangement and spacing. For the 4-to-1 symmetric combination in a uniform focusing channel, δf is given by

$$\delta f = -\frac{3}{4}+\log\{(\frac{1}{4})[2(\frac{\delta}{a})^2+1]^2(\frac{a}{\delta})^3\}$$

where δ is the beamlet displacement from the center and the a is the envelope radius of a beamlet.

Obvious reductions in the space-charge-generated emittance can be achieved when the beam separation and beam envelope radius are reduced. Since the beam size in equilibrium is proportional to the square root of the external focusing field, the reduction is size is probably not feasible unless some clever design of combiner focal elements which evades breakdown limits is introduced. In this study, the focusing field strength is assumed to be fixed. Reduction of the beam-separation is limited in order not to increase the field aberration near tbe electrodes and to provide a space for the chromatic aberration. Thus clearance of roughly 2 mm from the electrode surface must be maintained in a combiner.

The predicted increases in emittance can only be tested in a particle code or in a real experiment, due to various aberrations, breakdowns, and particle loss.

The numerical code HIBEAM, similar to the previous 2-D PIC code SHIFT, is used to test the geometric and chromatic aberration effects in a combiner, as well as sensitivity to the initial conditions.

4 Aberrations

4.1 Chromatic aberration of the centroid

The chromatic aberration of the centroid is minimized by selecting a first order achromatic combiner design. Such a design includes a minimum of four

bends in addition to the regular quadrupoles (or in conjunction with combined-function quadrupoles) to cancel the dispersion and its derivative at the end of the combiner as well as achieve the design displacement of the orbit.

The actual displacement from the design orbit is calculated by [2],

$$\frac{d^2D}{ds^2} = \frac{E'}{2V}D + \frac{E}{2V}(1 - \frac{V}{V_0})$$

where D is the displacement from the design orbit, $E'(s)$ is the quadrupole field gradient, $E(s)$ is the bend field, and V and V_0 are the cumulative voltage of the actual beam and its design value. By choosing bend strength (E) at four bends, both D and D' can be brought to zero at the combiner output.

A critical design constraint is keeping the pole tip electric field below the breakdown limit. This is particularly important since the upstream lattice is already optimized to use its maximum field within a safety factor of two.

4.2 Field aberrations

As the beamlets are brought together the space available for the electrodes becomes smaller, and the ratio of the electrode radius to the aperture radius deviates from the ideal ratio which the elimination of the dodecapole aberration. It is straightforward to calculate the three dimensional field decomposition of realistic quadrupole electrodes using the capacity matrix technique [3].

In a symmetric combiner, a simple cylindrical electrode quadrupole generates a strong dodecapole($M_{6,6}$) component which causes large emittance growth. Edge-shaped electrodes were introduced to eliminate dodecapoles in combiner quadrupoles, but they substantially increased the unwanted 20-pole($M_{10,10}$) component.

In a stonehenge combiner, "wire-cage" quadrupoles are needed to eliminate all the unnecessary multipoles although they are technically more difficult and complicated for both mechanical structure and voltage regulation.

5 Stonehenge combiner

The stonehenge beam configuration requires the last element of the combiner to be a combined function quadrupole. Furthermore, the last quadrupole is made of many wires nested in the narrow clearance between beams. The stonehenge combiner under study consists of four combined function quadrupoles and one regular quadrupole. The choice of the combined function elements is to reduce the number of elements in the combiner design and to make room for other special elements, such as auxiliary bends for beam steering and the beam scraper. On the other hand, since the field strength increases (because the bend and quadrupole fields add) extra care as to electrical breakdown is needed.

The schematic diagram of the combiner is displayed in Figure 4 where x-plane beam centroid trajectories at various beam energies and their dispersion are displayed. The beam-edge to beam-edge separation is reduced to 5 mm and the deviation from the design orbit is less than ± 1 mm for a momentum spread of ± 10 percent. This small chromatic aberration at the end of the combiner is due to second and higher order effects which departs from the first order achromat design. The design energy is somewhat less than that of the center of the beam pulse; this strategy produces an overall optimum, since the second and third order chromatic aberrations have opposite parity with respect to momentum tilt.

Since controlling the centroid orbit is most critical in terms of emittance growth, the dipole contributions from the beam-beam interaction to the design orbit, and the dispersion, have been compensated by adjusting the external bend strength at various locations. The quadrupole contribution to the beam-beam interaction is not significant; thus no quadrupole readjustment is made.

The matching section is located between the combiner and the down stream magnetic transport lattice. The lattice period of the combiner and downstream lattice is assumed to be 1.0 meter with effective quadrupole occupancy of 0.5. No longitudinal acceleration is assumed. The constant line charge density of $0.25\mu C/m$ for each of the four beamlets is also assumed regardless of their velocity.

The upstream lattice aperture (r_a) and quadrupole rod radius(r_r) are determined from the simple clearance prescription,

$$r_a = 1.25\,a + 1.0\,(cm)$$

$$r_r = (8/7)r_a$$

where a is the major radius of the matched beam. Since the major and minor radii of the matched beam envelope in the upstream lattice are given by (2.61730, 1.52249) cm, the aperture and the rod radii are determined to be (4.271625, 4.881857) cm.

Assuming a beam edge-to-edge separation distance of 5 mm at the end of the combiner, the (horizontal, vertical) centroid displacements of the design orbits of the beamlets are determined to be (1.77249, 4.33536) cm. Then the dimensions and field parameters of the "wire-cage" quadrupoles in a combiner are readily determined. (See table 1). Typical field line plots for the stonehenge combiner "wire-caged" quadrupoles are given in Figure 5.

The matching section following the combiner consists of five quadrupoles in which the merged beam is rematched into the downstream lattice. Since the emittance is rapidly changing in the matching section, conventional matching with an assumed constant emittance would result in a fractional mismatch as large as $\pm 20\%$. However, the emittance increase due to the envelope mismatch is negligibly small compared with that due to space charge, partly due to the

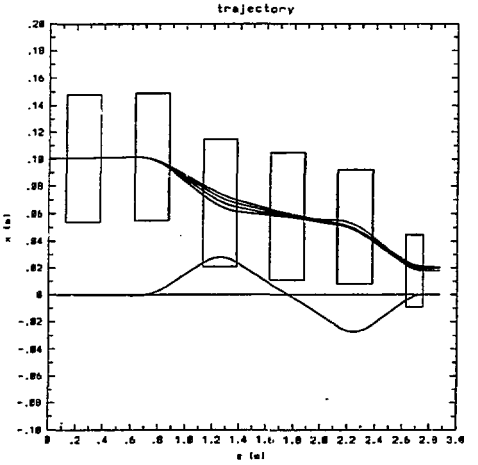

Figure 4: Schematics of stonehenge combiner. The upper four lines are the design orbit at 4 MeV (the one with minimum displacement at the end), and the centroid trajectory of the beam at 3.6, 4.4 and 4.8 MeV. Notice that horizontal and vertical scales are quite different in the figure.

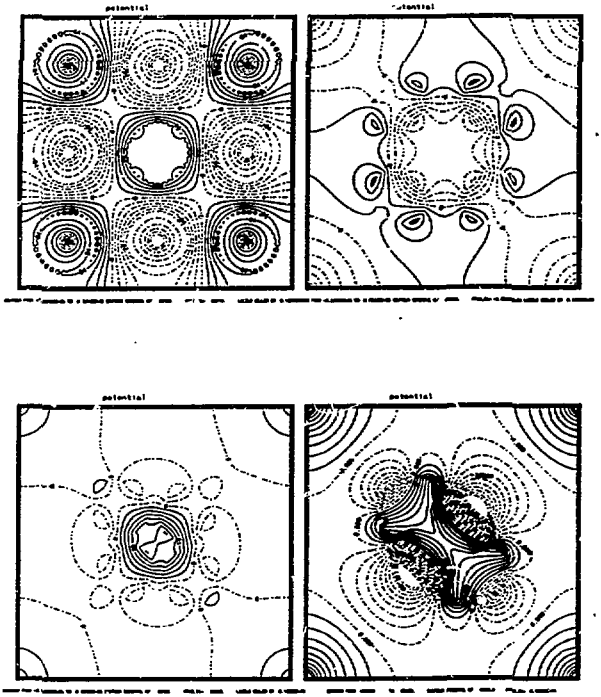

Figure 5: Potential plots for quadrupoles Q0(top left, F), Q1(top right, D+B), Q2(bottom left, F-B), and Q5(bottom right, D-B) for stonehenge combiner. All the figures are rotated 45° counter-clock wise.

round conducting boundary condition used; elaborate re-matching is omitted in the study.

The downstream lattice is assumed to consist of magnetic quadrupoles with aperture radius of 8 cm and period of 1 m.

No acceleration or compression is considered throughout the combiner; although the velocity tilt may be ±10% the combiner is short enough to neglect longitudinal effects.

5.1 "Wire" cage

The most critical element in a stonehenge combiner is the last quadrupole in a "wire cage" configuration.[2] Only an electric element is considered here because it is always cheaper but a magnetic version could be utilized at somewhat larger beam separations if the electric element's electrical break-down risk becomes severe. Beam dynamics calculations would be modified and some changes in quadrupole strengths would be needed to achieve achromaticity.

Assuming the wires are made of a stiff material such as Tungsten in order to have bending strength sufficient to be cantilevered from one side, the mechanical requirement can be easily calculated from the the field stress. The space charge effect is negligible.

Assuming a straight section of the wire has diameter 1 *mm* and length 10 *cm*, the maximum bending deflection is estimated to be less than 0.25 *mm*. The rest of the wire can be made of large diameter, with an extra jacket of Tungsten, or tapered, which gives firm support to the last straight section.

Since the electrical field is rather large, of order 60 kV/cm, special care as to the breakdown, such as scraping off the beam halo before the last element, should be used. The peak local field near the wire could be as large as 100 kV/cm.

Fortunately, the local peak field appears at the outer wires where wire-to-wire separation and the diameter of the wires can be made large. In addition, these wires do not have to be cantilevered because beams are merged to the center giving clear opening at the outer region.

For inside wires the field is roughly $20kV/cm$ which is a factor three less than at the outer wires. However, since the wires are cantilevered, the peak field at the tip of the wire could be much larger and some further study is needed.

Since the potential differences between adjacent wires are rather small for the inside wires, the field strength inside of the triangular region between the quadrupoles is much smaller.

Figure 6 shows the potential plots of a combined function "wire" quadrupole and expanded views of three strategic locations.

Since the field near the wire is not linear, the beams close to the wires are subject to the field aberrations. Figure 7 shows the magnitude of the field error

[2]Most of the last element concept is originated from A. Faltens' earlier consideration.[4]

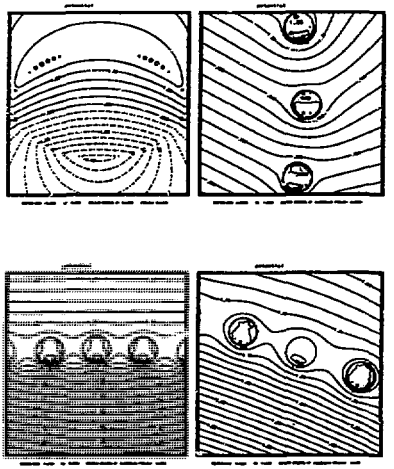

Figure 6: Potential plots of the combined function "wire" quadrupole. Full view of an quadrupole and the expanded view showing wires at right, top, and the middle locations on the aperture rim. The full size of the plot frame on the expanded view is 6 mm and the wire diameter is 1 mm.

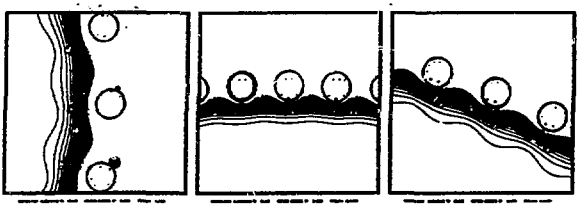

Figure 7: Field error contour plots of "wire" quadrupole at various locations. The contour interval corresponds to a 2 *mrad* deflection from the design orbit.

from the ideal combined function quadrupole.

The interval corresponds to a 2 *mrad* deflection angle from the design orbit for a particular design under study. From the downstream expected transverse thermal spread, a tolerable deflection angle may be 2 *mrad*, thus the last plotted line from the wire represents the clearance boundary from the beam to the wire. The beam clearance distance from the wire is mainly determined by the wire diameter, separation distance and applied voltage.

Since the potential difference between the wires could be as high as 100 *kV* some smoothly shaped braizing at the base of the wire to the insulator interface (in order to increase the breakdown distance along the insulator surface) may be used. Alternatively, if the breakdown risk becomes severe, pulsed quadrupoles could be used (as suggested by A. Faltens).

The bend and quadrupole field strengths from the "wire" quadrupoles are determined from the actual field calculation and the multipole decomposition using the code MULTI.

5.2 HIBEAM computation

Numerical verification follows the conceptual design. The HIBEAM code is adapted to the stonehenge configuration. The wires are represented by uniform charge densities instead of the actual conductors at constant potentials. The induced charge density along the wires is calculated using a capacity matrix technique where the required potential is specified at the rod boundary. This introduces small unimportant errors in fields near the wires as confirmed by the exact calculation (from the previous subsection) of the near fields of wires.

Due to flux leakage between the wires and the finite size of the wires the field generated is slightly different from the the desired design values; the computed

centroid trajectory does not exactly coincide with the design orbit. However, the difference at the end of the combiner is minimized due to the first order achromatic design.[3]

From the phase space plot (Figure 8) at the end of the combiner, at $z = 2.75\ m$, the converging angle is less than 5 $mrad$ and the separation distance of 5 mm has been achieved in the design without too much geometric aberration.

After the combiner, the beams are merged as indicated, with an increase of rms emittance (Figure 9). Most of the runs were made with 512×512 mesh points in a $40cm \times 40cm$ computation region and 16,000 macro particles were used. At the end of the combiner, mesh rezoning was performed to increase the resolution to 0.5 $mm/mesh$. A further increase in mesh(1024×1024 with rezone) and up to 64,000 particles were used but generated no noticeable change in final emittance.

The small initial decrease of the emittance is due to the rearrangement of the phase space due to the external focusing field of the matching section. Then the space charge equilibration takes place within one plasma period, where the emittance increases substantially at the expense of the field energy. The equipartition process appears in 10 meters, corresponding to roughly three plasma period, where the beam settles down to a new quasi-equilibrium. Due to the violent process involved, matching of the beam can not be quite accurate and the rms envelops shows a large mismatch (Figure 9). Although the mismatch does not introduce further emittance growth in this calculation, better matching could be used, if desired.

From the phase space scatter plot, some halo formation is observed; it comes from the overshoot of the edge particles, which were initially pushed by the space charge force to fill the gaps between the beams. As these energetic particles move back and forth in the merged beam, halo-like particles appear and disappear in configuration space at the undepressed tune frequency.

Since the wall radius was assumed to be 8 cm, which is relatively close to the beam and the halo formation, a small fraction of particles (0.15 %) are lost after the combiner.

As the energy of the beam could vary by as much as ±20 % in a single bunch in the ILSE design, the achromatic design of the combiner will produce centroid deviation (chromatic aberration) of up to 1 mm. The achromatic design was tested again with the HIBEAM PIC code and found in reasonable agreement with 1-D calculations for design.

Figure 10 shows that the final emittance vs. energy variation with energy variation of as large as ±20% is acceptable in the combiner design for the given line charge density of 0.25 $\mu C/m$ per beamlet. The sharp increase of the emittance at high and low energy end is obviously due to the beam getting too close to the wires, and the small decrease of the emittance at $v/v0$=1.1 is mainly due to the smaller separation among beams. The minimum of the emittance does

[3]This could be rectified when a better prescription of the potential at the wires is used.

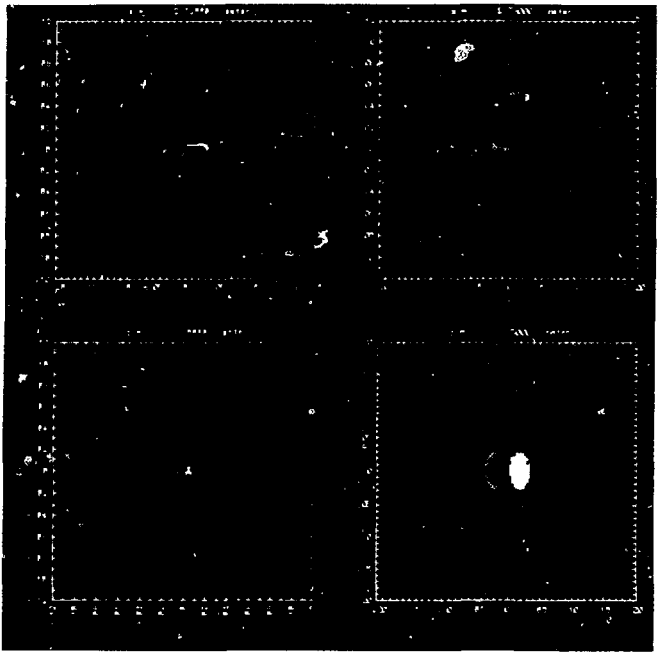

Figure 8: Phase space plots at the end of stonehenge combiner.

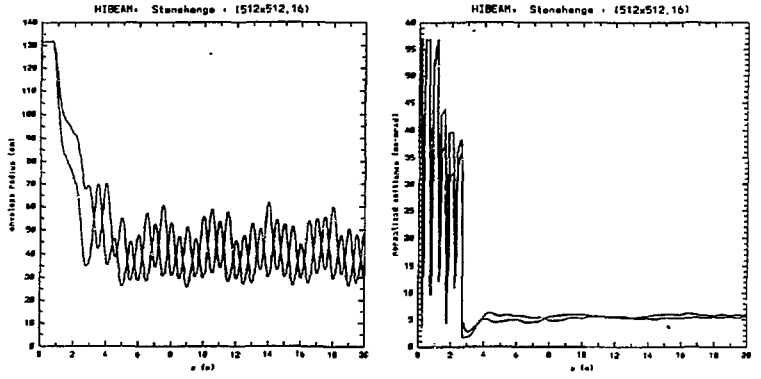

Figure 9: Rms envelope radii and normalized emittance versus z.

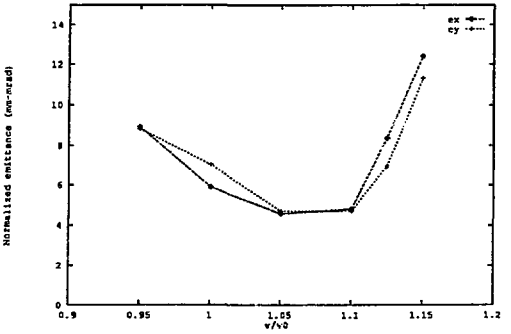

Figure 10: Final emittance vs. fractional velocity

not coincide with the design energy, mainly because of field leakage between the wires, thus the design orbit was not completely attained, and partly because of the matched envelop variation due to the energy tilt.

Using HIBEAM, the sensitivity on the initial position and the angle errors just before the combiner was examined by changing one beam parameters. Generally good position and angle tolerances of $\pm$ 1 *mm* and $\pm$ 5 *mrad* without emittance degradation were found. This suggests that rough steering before the combiner with this accuracy could be utilized if necessary.

6 Symmetric combiner

In the initial symmetric combiner design, simple quadrupoles made of cylinders were used. However, this generates unwanted dodecapole components of a few percent at the beam edge[5]. The combiner with simple cylindrical electrodes showed a strong field aberration effect on the beam dynamics and resulted in higher final normalized emittance. The dodecapole was eliminated using edge shaped electrodes, but introduced a large 20-pole component. The numerical calculation results for the combiner made of both simple cylindrical and edge shaped electrodes are reported here.

The basic symmetric combiner concept (after Lee and Judd's[2] design) consists of seven quadrupoles and three bends and one combined function element. The schematic of the design is shown in Figure 11, where the beam centroid

orbit and the dispersion are plotted.

If the quadrupoles are made of cylindrical electrodes, then the design is complete and the potential plots at various stage are readily obtained (Figure 12 and Table 2). The ratio of aperture to rod radius was varied somewhat in order to minimize the field aberration: no major improvement in emittance was observed. This is because when the aperture is increased for a given beam center-to-center distance, the dodecapole field error increases but the image force decreases, *i.e.* there are offsetting effects.

A combined function-quadrupole, made of cross-shaped plane ($4mm$ thick) and cylindrical electrodes (see Figure 12) at different potentials, is used at the end of the combiner to focus and bend in order to reduce the geometric phase space dilutions by reducing the envelope slope and space charge contribution by increasing the packing ratio. Due to the finite size of the last quadrupole, an additional small increase in final emittance is noted.

The effect of the dodecapole field aberration on the emittance is rather large, comparable to that of space charge; and complicated phase space deformation and even particle loss are observed. The final normalized emittance is 12 $mm - mrad$, which is 50 % larger than simple estimation from the space charge contribution alone and is about two times larger than that of the stonehenge combiner. Figure 13 shows the time history of the normalized emittance in the combiner and the following matching section. The large emittance immediately after the combiner represents the field aberration effect; a further increase of emittance in the matching section is mainly due to the space charge. Figure 14 shows the phase space plot at the end of the combiner. The square beam shape in configuration space is mainly due to the dodecapole field in the combiner. This deformation of the beam shape causes a small (2.5 %) particle loss at the last element of the combiner.

In an attempt to reduce the field aberration, edge-shaped electrodes were introduced (Figure 15). When the length of the edge is 0.542 times the aperture radius, defined by the square root of the inner square area, the dodecapole ($M_{6,6}$) component vanishes. However, a strong 20-pole component develops which could be dangerous to the beam dynamics ($M_{10,10}$=-0.0378).

HIBEAM computations are performed using edge-shaped quadrupoles and show no improvement on the emittance compared with the combiner quadrupoles using simple cylindrical electrodes. Figure 16 shows the field line plot of the rectangular quadrupoles. The thickness of the sheet electrode is chosen to be 4 mm, the same as that of the last combined function quadrupole. The quadrupole voltage is somewhat higher than for the cylindrical quadrupoles since a larger aperture is available in this geometry and the field gradient is assumed to be same.

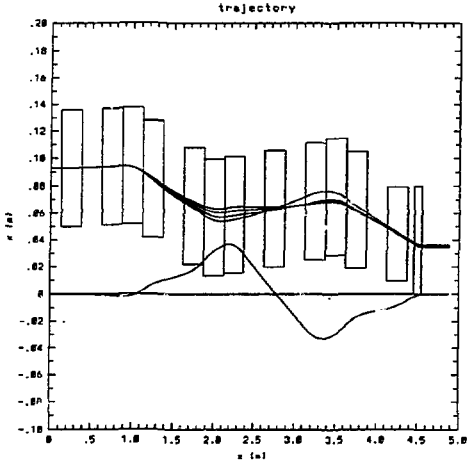

Figure 11: Schematics of symmetric combiner

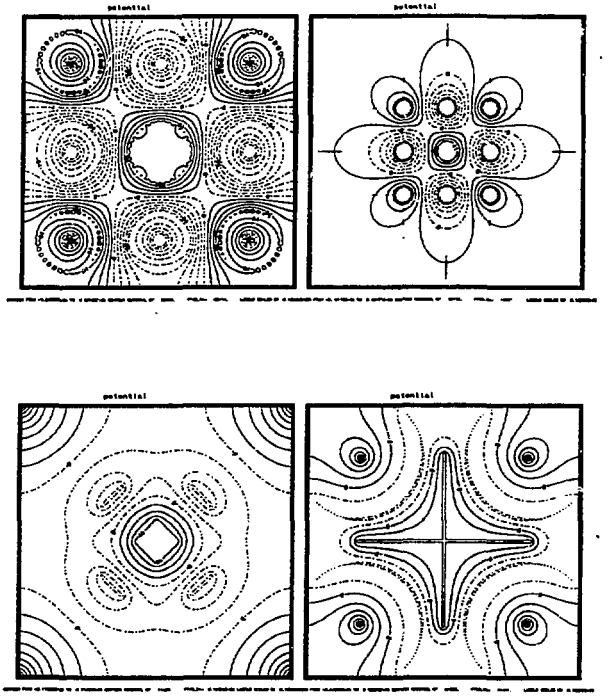

Figure 12: Potential plots of the upstream quadrupole(Q0), the last simple quadrupole(Q7), the bend(B2), and the combined function quadrupole.

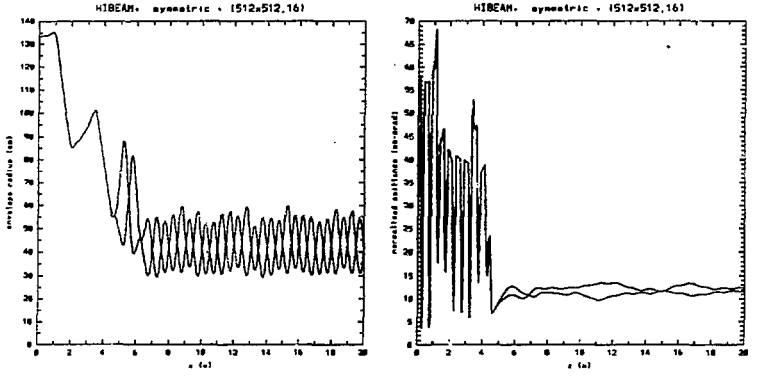

Figure 13: Rms envelope radii and normalized emittance versus z.

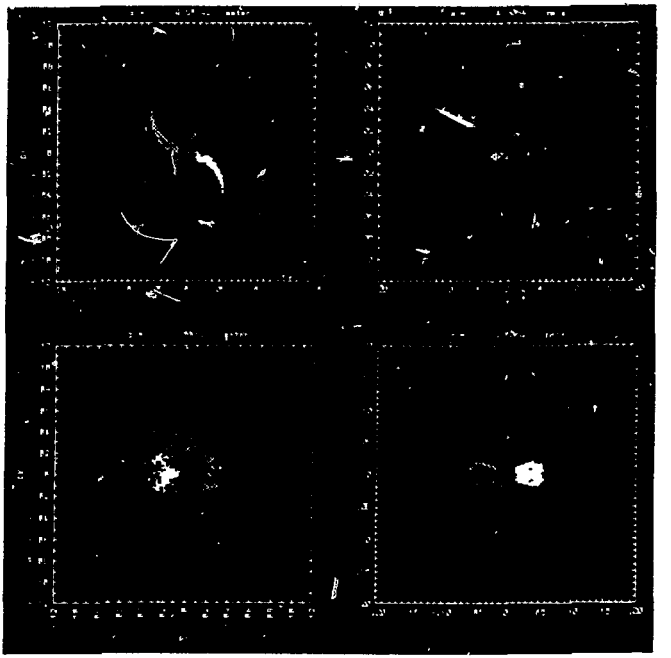

Figure 14: Phase space plots at the end of symmetric combiner.

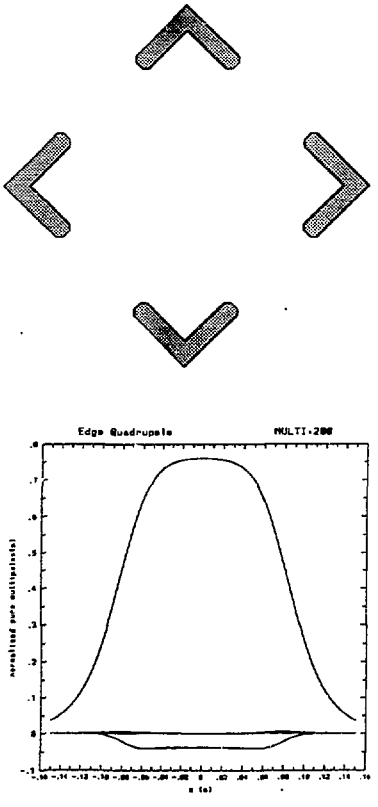

Figure 15: Edge-shaped electrode quadrupole and its multipoles ($M_{2,2}$, $M_{6,6}$, and $M_{10,10}$). The length of the electrode is approximately a half (0.542) of the aperture for the elimination of the dedecapole.

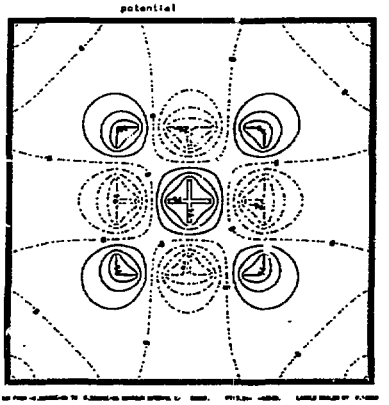

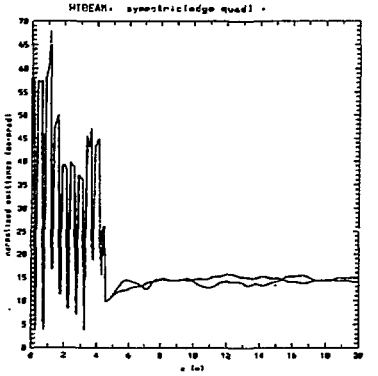

Figure 16: Potential plot from the rectangular quadrupole(Q4) in a symmetric combiner and history of its rms emittance.

7 Summary

The combiner concept is one of the most important options in a HIF driver which could reduce its cost by reducing the transverse dimensions of the system. In this ILSE design study, important aspects of the combiner are discussed: the emittance growth, reduction of the geometric and chromatic aberrations, and the technical and engineering difficulties. From the point of view of emittance growth the stonehenge combiner concept yields least increase, however, at the expense of technical difficulties such as breakdown and complexity of the "wire" cage geometry. These technical difficulties should be resolved by component development and operational experience, although they appears to be reasonably acceptable. The PIC code caiculation verified that the chromatic aberration can be controlled (up to $E/E_0 = \pm.15$) and that the tolerances for the position and the angle errors of the beams are less than 1 *mm* and 5 *mrad* respectively.

A symmetric combiner generates a rather large emittance than the stonehenge but the elements used are readily available.

Although in a HIF driver the momentum tilt is not as large as considered for ILSE, achromatic combiner design may be attractive despite the expense of a minimal increase of complexity since more bends are needed. Then the combiner for a driver looks very similar to the one considered except that the energy is about 10 times higher (at approximately 40 MeV) and the lattice period is three to four times longer. The same technical difficulty in terms of field strength and transverse space clearance is encountered. Since the length is longer, more mechanical support for the "wire" cage quadrupole might be needed. The expected emittance growth for the driver is less by the square root of the mass ratio, *i.e.* the heavier the ion, the less the final normalized emittance. Since the beam energy in a driver is much higher than ILSE the damage to the electrode from scrape-off is more severe and could cause further difficulty.

Only the four-to-one beam combination is considered in this study; many-to-one beam combinations need further consideration. The extreme of merging thousands of the beamlets was considered in a separate article.[6]

Acknowledgement

The author would like to thank E. Lee, A. Faltens, D. Judd for the useful discussions and the suggestions. D. Judd kindly edited the draft of many mistakes.

References

[1] K. D. Hahn and L. Smith, LBL-26167 and HIFAN-415, October, 1988.

[2] E. Lee, "ILSE combiner concept", HIFAR-311, July, 1991. E.P. Lee and D. L. Judd, "Combiner Studies", HIFAR-315, Sept., 1991.

[3] Kyoung Hahn, "Three dimensional multipole decomposition of fields" to be published in Nucl. Inst. and Meth. in Physics Research A. Martin Berz, William M. Fawley, and K Hahn, "High order calculation of the multipole content of the three dimensional electrostatic geometries", Nucl. Inst. and Meth. in Phys. Research A307 (1991) 1.

[4] A. Faltens, "Special elements for beam combining", HIFAR-163, Aug., 1987.

[5] K. Hahn, "ILSE symmetric combiner", HIFAR-391, Sep., 1993.

[6] K. hahn, "Electrostatic energy change form many beamlets to a uniform beam", HIFAR-388, Sep., 1993.

Table 1: Combined function quadrupole parameters for stonehenge combiner

	(Major, Minor) radii (m)	length (m)	E' (MV/m^2)	$E_{B_{(x,y)}}$ (MV/m)
Q1	(0.043, 0.033)	0.25	90.54	(1.902, 1.305)
Q2	(0.043, 0.033)	0.25	90.54	(1.493, 1.305)
Q3	(0.043, 0.033)	0.25	90.54	(0., 0.)
Q4	(0.042, 0.032)	0.25	90.54	(1.895, 1.250)
Q5	(0.0281, 0.0172)	0.25	90.54	(3.694, 2.377)

Table 2: Quadrupole and Bend parameters for symmetric combiner

	aperture (m)	rod radius (m)	length (m)	E' (MV/m^2)
Q0	0.043	0.0491	0.25	90.54
Q1	0.043	0.0415	0.25	90.54
Q2	0.033	0.0218	0.25	90.54
Q3	0.033	0.0152	0.25	90.54
Q4	0.033	0.0197	0.25	90.54
Q5	0.033	0.0251	0.25	90.54
Q6	0.033	0.0188	0.25	90.54
Q7	0.03	0.0091	0.25	90.54

	gap distance (m)	width (m)	axial length (m)	E_B (MV/m)
B1	0.043	0.0519	0.25	1.391
B2	0.033	0.0236	0.25	1.406
B3	0.033	0.0388	0.25	1.621